 doi:10.20944/preprints202103.0013.v1

Communication

Photonic microsphere-based temperature sensors with ZnO ALD coating – comparison study

Paulina Listewnik [1,*], Mikhael Bechelany[2], Małgorzata Szczerska[1,*]

[1] Department of Metrology and Optoelectronics, Faculty of Electronics, Telecommunications and Informatics, Gdańsk University of Technology, 11/12 Narutowicza Street, 80-233 Gdańsk, Poland; malszcze@pg.edu.pl (M.S.)

[2] Institut Européen Des Membranes, IEM, UMR 5635, Univ Montpellier, CNRS, ENSCM, 34095, Montpellier Cedex 5, France; mikhael.bechelany@umontpellier.fr (M.B.)

* Correspondence: pauliste@student.pg.edu.pl (P.L.); malszcze@pg.edu.pl (M.S.)

Abstract: This study presents the microsphere-based fiber-optic sensor with the ZnO ALD coating thickness of 100 nm and 200 nm for temperature measurements. Metrological properties of the sensor were investigated over the temperature range of 100°C to 300°C, with a 10°C step. The interferometric signal is used to control whether the microstructure is intact. Spectrum shift of a reflected signal is used to conclude changes in measured parameter for the sensor with a 100 nm coating, while the reflected signal intensity is an indicator during measurements executed by a sensor with a 200 nm coating. With changing temperature, the peak position or intensity of a reflected signal also changes. The R^2 coefficient of the presented sensors indicates a linear fit of over 0.99 to the obtained data. The sensitivity of the sensors, investigated in this study, equals 103.5 nW/°C and 0.019 nm/°C for ZnO thickness of 200 nm and 100 nm, respectively.

Keywords: temperature sensor, fiber optic sensor, photonic sensor; atomic layer deposition; microsphere; temperature; ZnO

1. Introduction

Fiber-optic sensors have been developed and improved upon for a few decades. Due to their versatility, they are used in numerous fields, such as industry, science or medicine [1–4]. Because of their many properties, such as chemical inertness or resistance to electromagnetic interference, they can often be utilized in places, where electric sensors cannot be applied, e.g., hazardous and combustible areas, severe climatic conditions and hard to access places [5–8]. Optimization of measurement parameters plays a significant role in the development of the fiber-optic sensors. While planning measurements, the selection of the sensor is a crucial element, depending on their purpose and conditions, in which they will be performed. There are many ways to tune measurement parameters and metrology properties of fiber-optic sensors.

Firstly, by modification of the sensor's structure. Advancements in technology and fabrication techniques – fiber-optic fusion splicers and laser splicing systems, femtosecond lasers, chemical etching [9–13] – allow to obtain a multitude of fiber-optic structures. Many of them, including microdiscs, microrings, tapers, microresonators and microspheres are coupled with a high coherent light source to generate resonance within the structure, on the basis of the Whispering Mode Gallery (WMG) phenomenon [14,15].

Another way to modify fiber-optic sensors is by addition of a coating on either the flat end-face of the fiber or on the surface of the structure. The coatings consist of a variety of materials, mostly 2D and they can be deposited in different forms. Based on their properties they are used for specific applications. For example, due to its structure, graphene oxide coating is ideal for humidity and refractive index measurements [16]. Single-walled carbon nanotubes (SWCNT) [17] are used for the

Preprints (www.preprints.org) | NOT PEER-REVIEWED | Posted: 1 March 2021 doi:10.20944/preprints202103.0013.v1

detection of ammonia, ethanol and methanol vapor, because of their interaction with the coating. The Pd-Au layer is used for hydrogen concentration sensing [18].

The deposition method of the coating is an important issue while modifying parameters of fiber-optic sensors. Whether the materials are deposited by dip-coating method, Atomic Layer Deposition or magnetron sputtering, the coatings adopt different geometry, shading and uniformity [19–24].

Based on the type of sensor, diversity of designs and parameters can be optimized: adjustable cavity length, structure modification [25–28], as well as metrological properties, such as: resolution, precision, sensitivity, accuracy [29,30]. Many researchers contribute to determining the properties and parameters of various materials and structures [31,32].

This study investigates the sensing abilities of the microsphere-based fiber-optic sensors with a 100 nm and 200 nm ZnO ALD coating during temperature measurements. By combining several methods of modification of the fiber-optic sensors, standalone devices can be obtained. This way, the complexity of the measurement system can be reduced and the range of adjustable parameters is widened. The ZnO sensor properties was investigated in the range of 100°C to 300°C. In this temperature range, ZnO is well known for it is chemical stability even under air. For this reason, ZnO is widely used for gas sensor applications for instance [33].

2. Materials and Methods

Measurements were performed using a sensor made of a standard single-mode telecommunication optical fiber (SMF-28, Thorlabs Inc., Newton, NJ, USA) with a microsphere structure produced at the end of the fiber, using a fiber-optic splicer (FSU975, Ericsson, Sweden). To obtain a microsphere with a diameter of 245 μm, splicing proceeded in three-step pull. The fiber-optic splicer uses an electric arc to melt the fiber, while the pulling causes a formation of a microsphere. By choosing accurate splicing parameters, such as time of pull, electric arc current, fiber distance, the process can be controlled to achieve a highly repeatable structure. After the manufacturing of the microsphere, the ZnO coating was deposited on its surface by Atomic Layer Deposition (ALD) method. ALD is a vapor phase deposition technique enabling the synthesis of ultrathin films with a sub-nanometer thickness control. A key-benefit of ALD is its high conformality. In fact, ALD can be used to coat complex 3D substrates with a conformal and uniform layer of high-quality materials, a capability unique amongst thin film deposition techniques. So, by using ALD, we were sure that ZnO will be uniformly and accurately grown on the microspheres inside the deposition Chamber [34]. A custom made ALD reactor was used for the synthesis of ZnO layers. ALD was performed using sequential exposures of Diethyl Zinc and H2O separated by a purge of nitrogen with a flow rate of 100 sccm. The deposition regime for ZnO consisted of 0.1 s pulse of DEZ, 20 s of exposure to DEZ, 40 s of purge with argon followed by 2 s pulse of H2O, 30 s of exposure to H2O and finally 60 s purge with argon. ZnO thin films with different number of cycles were deposited both on Si substrates and microsphere by ALD, the temperature was fixed to 100 °C [35,36]. After the deposition process, the sensor is connected to the optical coupler by fusion splicing.

To assess the quality of the structure and the deposited ZnO ALD coating of 100 nm thickness, it was then investigated under Scanning Electron Microscope (SEM, Phenom XL G2, Thermo Fisher Scientific, Waltham, MA, USA), which results are shown in Figure 1.

Preprints (www.preprints.org) | NOT PEER-REVIEWED | Posted: 1 March 2021 doi:10.20944/preprints202103.0013.v1

Figure 1. SEM image of the microsphere-sensor with a 100 nm ZnO ALD coating. Magnification of 1000x.

The image shows the device with a magnification of 1000x and it can be seen, the structure exhibits excellent roundness. Furthermore, the presence of ZnO coating is apparent.

The metrological properties of the sensor were validated by performing experimental measurements. The utilized setup, which consists of a light source, an optical spectrum analyzer, the developed sensor and a temperature calibrator, is presented in Figure 2.

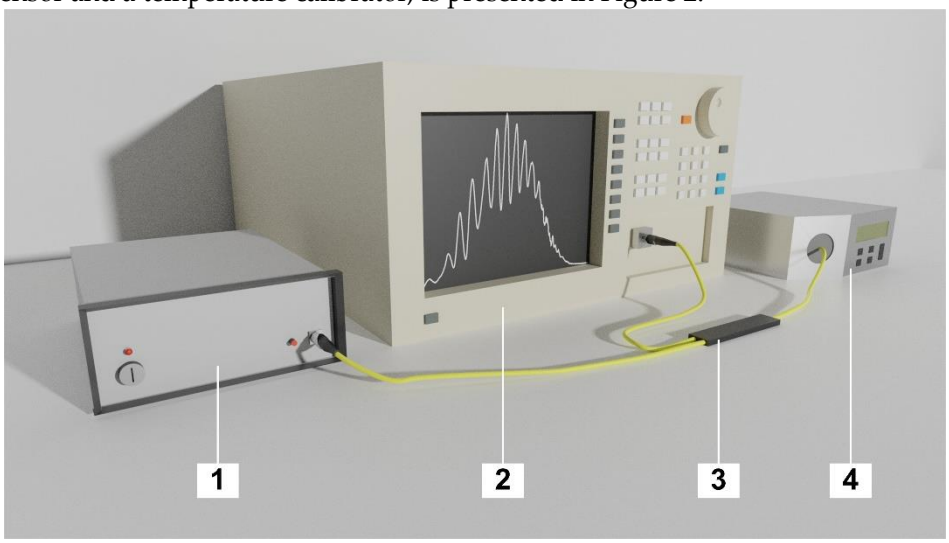

Figure 2. Experimental setup, where: 1 – light source, 2 – Optical Spectrum Analyzer, 3 – optical coupler, 4 – temperature calibrator.

During the investigation, the sensor is placed in the temperature calibrator (ETC-400A, Ametek, Berwyn, PA, USA), which was increased from 100°C to 300°C, with a 10°C step. The temperature was stabilized for 3 minutes, at each step, allowing the sensor to adjust to altered conditions. The measurements were executed using a light source with a center wavelength of 1310 nm ±20 nm (SLD-1310-18-W, FiberLabs Inc., Fujimino, Japan). The signal was propagated through a 2:1 50/50% optical coupler (G657A, CELLCO, Kobylanka, Poland) to the sensor head coated with a 100 nm ZnO ALD coating, which is highly reflective, allowing the wave to superpose, therefore inciting interference as shown in Figure 3.

Preprints (www.preprints.org) | NOT PEER-REVIEWED | Posted: 1 March 2021 doi:10.20944/preprints202103.0013.v1

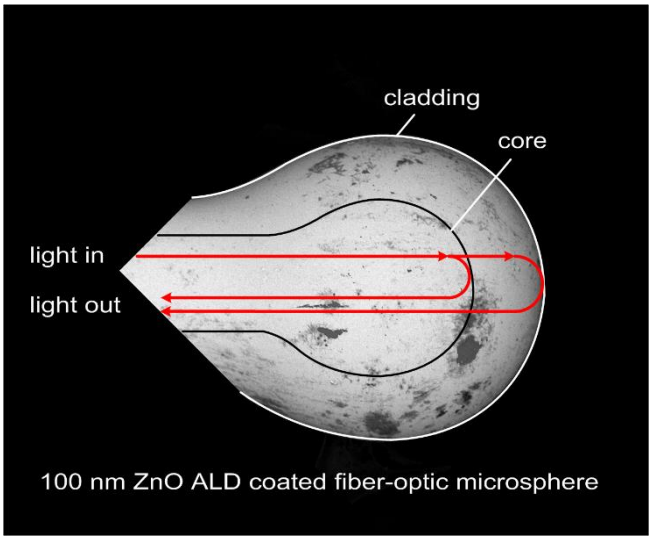

Figure 3. Principle of operation of a microsphere-based fiber-optic sensor.

By obtaining interference, the integrity of the structure can be monitored, ensuring the sensor is not damaged. The reflected signal is then collected by Optical Spectrum Analyzer (OSA, Ando AQ6319, Yokohama, Japan). Depending on the position of the spectral peak of the signal, the temperature can be determined.

3. Results and Discussion

This section presents results, which were acquired from the measurements performed with the setup shown above for the sensor with a 100 nm ZnO ALD coating. The detailed results of an investigation of the sensor with 200 nm coating are presented elsewhere [37]. This section also describes the comparison of the data sets obtained for both sensors.

Figure 4 shows normalized values of the measured signal response for the microsphere-based sensor with a 100 nm ZnO ALD coating, at 100°C and 300°C to preserve the readability of the plot. By rising the temperature, the spectral peak of the reflected signal shifts toward lower values of the wavelength. The envelope, however, remains similar for each temperature. In addition, interference fringes visible in Figure 4, inform about the integrity of the sensor head structure, which allows to monitor its condition in real-time.

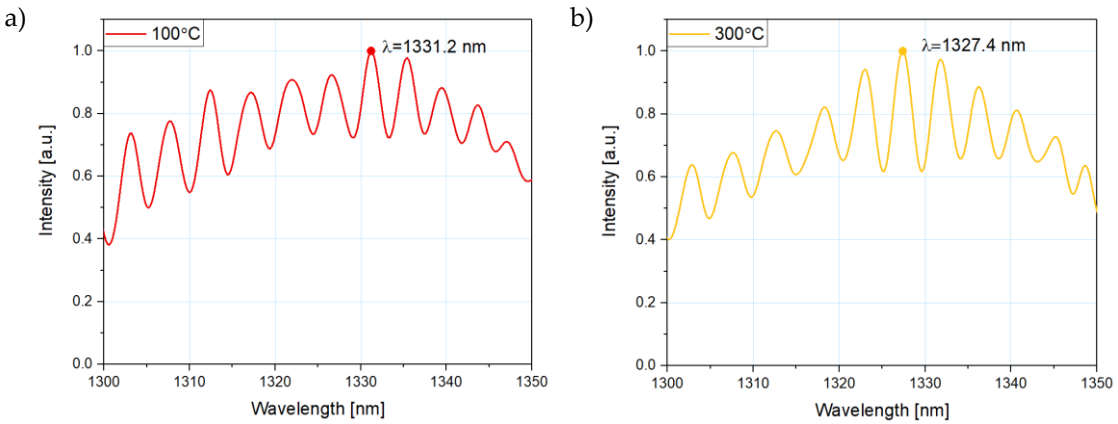

Figure 4. Normalized measured response of the reflected signal for the microsphere-based sensor with 100 nm ZnO ALD coating at a) 100°C and b) 300°C.

Preprints (www.preprints.org) | NOT PEER-REVIEWED | Posted: 1 March 2021 doi:10.20944/preprints202103.0013.v1

The dependence of the peak wavelength position on the temperature can be observed in Figure 5. Moreover, the theoretical linear fit is also presented, as well as coefficient R^2, which equals 0.991, was determined to confirm the fitness of the obtained data to the theoretical model. Furthermore, the results presented in Figure 5 allowed to calculate the sensitivity of the microsphere-based sensor with a 100 nm ZnO ALD coating – 0.019 nm/°C.

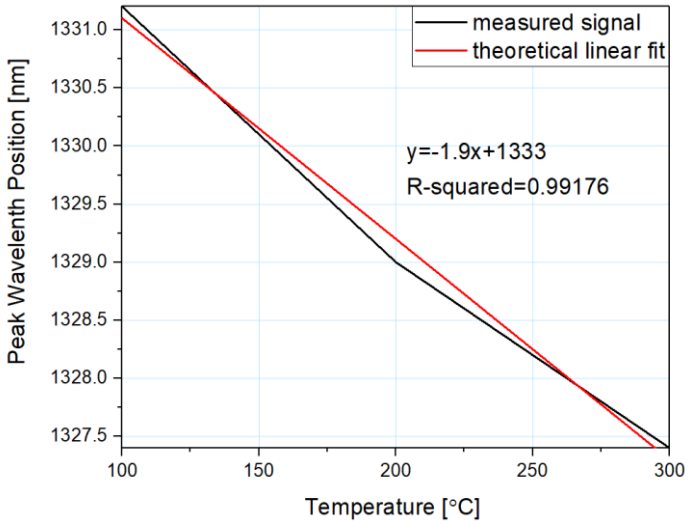

Figure 5. Dependence of the spectral shift of a reflected signal on the temperature.

The spectrum changes its peak wavelength position when the temperature is altered. As the temperature rises, the spectrum shifts by a constant value throughout the whole range of roughly 2 nm per 100°C. By following linear regression, it is possible to determine the position of the reflected signal peak for each measured temperature.

Beside peak wavelength shift, the sensor with a 100 nm ZnO ALD coating also retains the same property as a sensor with a 200 nm coating. The intensity of the reflected signal increases when the temperature rises. The dependence of the reflected signal's intensity on the temperature is presented in Figure 6.

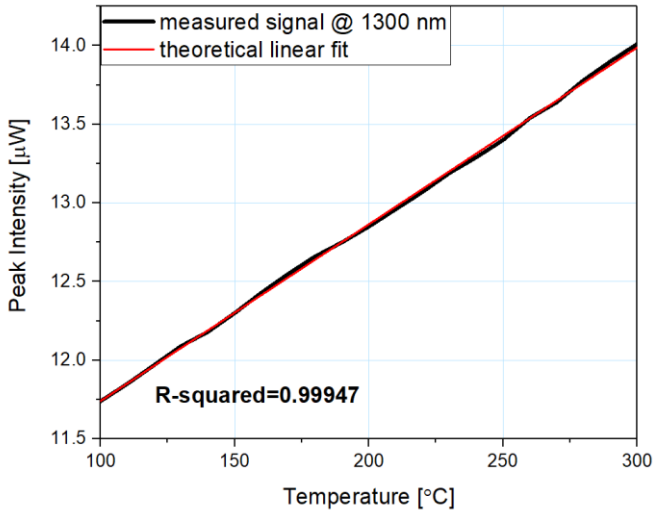

Figure 6. Reflected signal intensity dependence on the changing temperature and its theoretical linear fit, measured at a wavelength of 1300 nm, using the microsphere-based sensor with 100 nm ZnO ALD coating.

The results presented in Figure 6 allowed to calculate that the increase of the signal throughout the examined range is 16%. The sensitivity of the microsphere-based sensor with 100 nm ZnO ALD coating was also calculated and it equals 11.35 nW/°C. A theoretical linear fit was included in the

Preprints (www.preprints.org) | NOT PEER-REVIEWED | Posted: 1 March 2021 doi:10.20944/preprints202103.0013.v1

presented graph and the coefficient R^2=0.999 was determined to confirm the fitness of obtained data to the theoretical model.

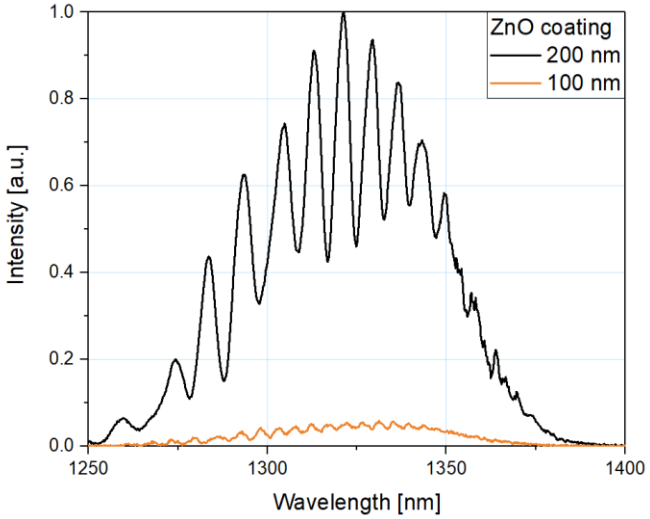

Figure 7. Normalized reflected spectra measured at 100°C with microsphere-based sensors with a 200 nm (black line) and a 100 nm (orange line) ZnO ALD coating.

Figure 7. shown measured reflected spectra for microsphere-based fiber-optic sensors with 100 nm and 200 nm ZnO ALD coating at 100°C. Normalization was performed to the highest value of intensity. It can be observed, the intensity of a sensor with a 200 nm coating is over 10 times higher than the intensity of a sensor with a 100 nm coating.

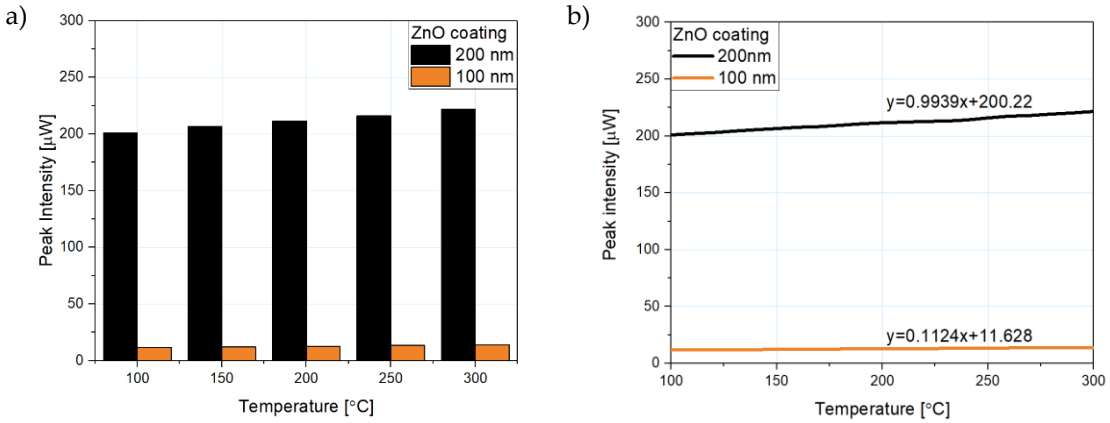

Figure 8. The dependency of the peak intensity on the temperature, where: a) comparison of the obtained peak intensity of the reflected signal for each sensor, b) obtained data and its linear approximation.

Figure 8(a) shows the dependency of the peak intensity on temperature for micro-sphere fiber-optic sensors and their difference while using 200 nm and 100 nm ZnO ALD coating. Figure 8(b) also shows their theoretical linear fit described by a linear function. Because the linear fit is a close match to the obtained data, by following linear regression, it is possible to accurately predict metrological properties of the sensor at a temperature beyond the investigated range and to forecast the behavior of the sensor with any other thickness of a ZnO ALD coating. By considering a slope of the function, the sensitivity of the sensor can be further estimated, whereas by analyzing their y-intercept, the intensity level can be estimated.

Preprints (www.preprints.org) | NOT PEER-REVIEWED | Posted: 1 March 2021 doi:10.20944/preprints202103.0013.v1

In addition, the values of linearity error, sensitivity error and approximation error were calculated. Their comparison in relation to both sensors is presented in Table 1. The data for a sensor with a 100 nm coating includes both spectral and intensity analysis, because the device provides two ways of measurement.

Table 1. Measurement parameters of the sensors.

Parameter	Sensor with a 100 nm coating		Sensor with a 200 nm coating
Investigated range	100°C – 300°C		
Analysis type	spectral	intensity	intensity
Sensitivity	0.019 nm/°C	11.35 nW/°C	103.5 nW/°C
Sensitivity error	0%	0.99%	3.97%
Theoretical sensitivity	0.019 nm/°C	11.24 nW/°C	99.39 nW/°C
Linearity error	5.2%	1.15%	5%
Approximation error	0.02%	0.2%	0.49 %

As mentioned before, the measurement properties of the microsphere-based sensors with ZnO ALD coatings of 100 nm and 200 nm were investigated in the temperature range of 100°C – 300°C. Based on acquired data, the sensitivity of the sensors as well as sensitivity error, determining a deviation of this parameter from the one fitted from the theoretical zero-deviation slope, were calculated respectively from the formulas (1) and (2):

$$S = \frac{\Delta I}{\Delta T}, \quad (1)$$

where: S – sensitivity of the sensor, ΔI – intensity of the reflected signal, ΔT – temperature range.

$$u_{sensitivity} = \left(1 - \frac{S_{theor}}{S}\right) * 100\%, \quad (2)$$

where: $u_{sensitivity}$ – sensitivity error, S_{theor} – theoretical fitting sensitivity.

While the sensitivity error of the sensor with a 100 nm coating is, at most, 1%, the sensor with a 200 nm coating errs by 3.97%. Throughout measurement planning it is worth to consider the sensitivity needed to accomplish a task. For investigations requiring lower sensitivity, the sensor with thinner ZnO ALD coating may still provide sufficient metrological parameters, whereas in terms of time and cost of its production, it will be more beneficial.

The dependence of the changes occurring in the spectra on increasing temperature during measurements with each sensor is consistent with linear characteristic and the linear fit was included in the graphs. Therefore, the uncertainty of the obtained data to the theoretical model was calculated (3):

$$u_{linearity} = \frac{\max|I - I_{theor}|}{\Delta I}, \quad (3)$$

where: $u_{linearity}$ – linearity error, I – intensity of the reflected signal, I_{theor} – theoretical fitting intensity.

As can be seen, the linearity error in terms of spectral analysis is almost 5 times lower for the sensor with a 100 nm coating. However, considering its linearity error by spectral analysis, it also deviates by 5%.

The next calculated parameter was approximation error, which indicates divergency between obtained data and its linear fit. For both presented sensors, approximation error is less than 0.5%. Approximation error was calculated from the following formula (4):

$$\delta = \left|\frac{\upsilon_M - \upsilon_R}{\upsilon_R}\right| * 100\%, \quad (4)$$

where: δ – approximation error, υ_M – obtained data, υ_R – linear fit.

4. Conclusion

Microsphere-based sensors are ideal for long-term and remote measurements of parameters such as temperature or refractive index due to their ability to constantly monitor the integrity of the

sensor head, therefore limiting uncertainty of inaccurate measurements, which allows to perform undisturbed measurements. The presented study investigates measurement parameters of a 100 nm ZnO and a 200 nm ALD coatings on the surface of a microsphere-based fiber-optic sensor for temperature measurements. While devising the measurements, it is important to select the proper parameters of the fiber-optic sensor coating for optimal efficiency. Presented sensors exhibit a close match between measurement data and theoretical linear fit, which is confirmed by an R^2 coefficient of over 0.99. The sensitivity of the sensor with a 100 nm coating equals 0.019 nm/°C, while the sensitivity of the sensor with a 200 nm coating equals 103.5 nW/°C. Additionally, for the microsphere-based sensor with 100 nm ZnO ALD coating, changes of temperature can be observed based on the intensity increase, which coincides with the rise of the temperature. The sensor also indicates its proper operation by appearance of interference. By introducing the interference signal into measured spectra, the sensors are able to indicate their proper operation. In case of interference signal presence, information about the integrity of the microstructure is provided.

Funding: This research was funded by the Polish National Agency for Academic Exchange—NAWA under bilateral exchange of scientists between France and Poland PHC Polonium (PPN/BFR/2019/1/00005). Financial support of these studies from Gdańsk University of Technology by the 11/2020/IDUB/I.3/CC grant under the Curium Combating Coronavirus and by the 8/2020/IDUB/III.4.1/Tc grant under Technetium Talent Management Grants - EIRU programs is gratefully acknowledged. The author acknowledges the financial support of the DS Programs of the Faculty of Electronics, Telecommunications and Informatics of the Gdańsk University of Technology.

Conflicts of Interest: The authors declare no conflict of interest.

References

1. Xiong, F.B.; Sisler, D. Determination of Low-Level Water Content in Ethanol by Fiber-Optic Evanescent Absorption Sensor. *Optics Communications* **2010**, *283*, 1326–1330, doi:10.1016/j.optcom.2009.11.075.
2. Ramakrishnan, M.; Rajan, G.; Semenova, Y.; Farrell, G. Overview of Fiber Optic Sensor Technologies for Strain/Temperature Sensing Applications in Composite Materials. *Sensors (Basel)* **2016**, *16*, doi:10.3390/s16010099.
3. Karpienko, K.; Wróbel, M.S.; Jedrzejewska-Szczerska, M. Determination of Refractive Index Dispersion Using Fiber-Optic Low-Coherence Fabry–Perot Interferometer: Implementation and Validation. *Opt. Eng* **2014**, *53*, 077103, doi:10.1117/1.OE.53.7.077103.
4. Witt, J.; Narbonneau, F.; Schukar, M.; Krebber, K.; De Jonckheere, J.; Jeanne, M.; Kinet, D.; Paquet, B.; Depre, A.; D'Angelo, L.T.; et al. Medical Textiles With Embedded Fiber Optic Sensors for Monitoring of Respiratory Movement. *IEEE Sensors J.* **2012**, *12*, 246–254, doi:10.1109/JSEN.2011.2158416.
5. Tripathi, S.M.; Bock, W.J.; Mikulic, P. A Wide-Range Temperature Immune Refractive-Index Sensor Using Concatenated Long-Period-Fiber-Gratings. *Sensors and Actuators B: Chemical* **2017**, *243*, 1109–1114, doi:10.1016/j.snb.2016.12.012.
6. Hromadka, J.; Mohd Hazlan, N.N.; Hernandez, F.U.; Correia, R.; Norris, A.; Morgan, S.P.; Korposh, S. Simultaneous in Situ Temperature and Relative Humidity Monitoring in Mechanical Ventilators Using an Array of Functionalised Optical Fibre Long Period Grating Sensors. *Sensors and Actuators B: Chemical* **2019**, *286*, 306–314, doi:10.1016/j.snb.2019.01.124.
7. Li, M.; Dubaniewicz, T.; Dougherty, H.; Addis, J. Evaluation of Fiber Optic Methane Sensor Using a Smoke Chamber. *International Journal of Mining Science and Technology* **2018**, *28*, 969–974, doi:10.1016/j.ijmst.2018.05.010.

8. Kou, J.; Feng, J.; Ye, L.; Xu, F.; Lu, Y. Miniaturized Fiber Taper Reflective Interferometer for High Temperature Measurement. *Opt. Express* **2010**, *18*, 14245, doi:10.1364/OE.18.014245.
9. Duan, D.-W.; Rao, Y.; Hou, Y.-S.; Zhu, T. Microbubble Based Fiber-Optic Fabry–Perot Interferometer Formed by Fusion Splicing Single-Mode Fibers for Strain Measurement. *Appl. Opt.* **2012**, *51*, 1033, doi:10.1364/AO.51.001033.
10. Zhang, L.; Jiang, Y.; Jia, J.; Wang, P.; Wang, S.; Jiang, L. Fiber-Optic Micro Vibration Sensors Fabricated by a Femtosecond Laser. *Optics and Lasers in Engineering* **2018**, *110*, 207–210, doi:10.1016/j.optlaseng.2018.06.003.
11. Zhang, Y.; Yuan, L.; Lan, X.; Kaur, A.; Huang, J.; Xiao, H. High-Temperature Fiber-Optic Fabry–Perot Interferometric Pressure Sensor Fabricated by Femtosecond Laser. *Opt. Lett.* **2013**, *38*, 4609, doi:10.1364/OL.38.004609.
12. Cardona-Maya, Y.; Villar, I.D.; Socorro, A.B.; Corres, J.M.; Matias, I.R.; Botero-Cadavid, J.F. Wavelength and Phase Detection Based SMS Fiber Sensors Optimized With Etching and Nanodeposition. *Journal of Lightwave Technology* **2017**, *35*, 3743–3749, doi:10.1109/JLT.2017.2719923.
13. Coelho, L.; Almeida, J.M.M.M. de; Santos, J.L.; Viegas, D. Fiber Optic Hydrogen Sensor Based on an Etched Bragg Grating Coated with Palladium. *Appl. Opt., AO* **2015**, *54*, 10342–10348, doi:10.1364/AO.54.010342.
14. Liang, L.; Li, M.; Liu, N.; Sun, H.; Rong, Q.; Hu, M. A High-Sensitivity Optical Fiber Relative Humidity Sensor Based on Microsphere WGM Resonator. *Optical Fiber Technology* **2018**, *45*, 415–418, doi:10.1016/j.yofte.2018.07.023.
15. Ma, Q.; Rossmann, T.; Guo, Z. Whispering-Gallery Mode Silica Microsensors for Cryogenic to Room Temperature Measurement. *Meas. Sci. Technol.* **2010**, *21*, 025310, doi:10.1088/0957-0233/21/2/025310.
16. Dissanayake, K.P.W.; Wu, W.; Nguyen, H.; Sun, T.; Grattan, K.T.V. Graphene-Oxide-Coated Long-Period Grating-Based Fiber Optic Sensor for Relative Humidity and External Refractive Index. *Journal of Lightwave Technology* **2018**, *36*, 1145–1151, doi:10.1109/JLT.2017.2756097.
17. Manivannan, S.; Saranya, A.M.; Renganathan, B.; Sastikumar, D.; Gobi, G.; Park, K.C. Single-Walled Carbon Nanotubes Wrapped Poly-Methyl Methacrylate Fiber Optic Sensor for Ammonia, Ethanol and Methanol Vapors at Room Temperature. *Sensors and Actuators B: Chemical* **2012**, *171–172*, 634–638, doi:10.1016/j.snb.2012.05.045.
18. Westerwaal, R.J.; Rooijmans, J.S.A.; Leclercq, L.; Gheorghe, D.G.; Radeva, T.; Mooij, L.; Mak, T.; Polak, L.; Slaman, M.; Dam, B.; et al. Nanostructured Pd–Au Based Fiber Optic Sensors for Probing Hydrogen Concentrations in Gas Mixtures. *International Journal of Hydrogen Energy* **2013**, *38*, 4201–4212, doi:10.1016/j.ijhydene.2012.12.146.
19. Barranco, A.; Borras, A.; Gonzalez-Elipe, A.R.; Palmero, A. Perspectives on Oblique Angle Deposition of Thin Films: From Fundamentals to Devices. *Progress in Materials Science* **2016**, *76*, 59–153, doi:10.1016/j.pmatsci.2015.06.003.
20. Brinker, C.J. Dip Coating. In *Chemical Solution Deposition of Functional Oxide Thin Films*; Schneller, T., Waser, R., Kosec, M., Payne, D., Eds.; Springer Vienna: Vienna, 2013; pp. 233–261 ISBN 978-3-211-99310-1.
21. Grosso, D. How to Exploit the Full Potential of the Dip-Coating Process to Better Control Film Formation. *J. Mater. Chem.* **2011**, *21*, 17033, doi:10.1039/c1jm12837j.

22. Johnson, R.W.; Hultqvist, A.; Bent, S.F. A Brief Review of Atomic Layer Deposition: From Fundamentals to Applications. *Materials Today* **2014**, *17*, 236–246, doi:10.1016/j.mattod.2014.04.026.
23. George, S.M. Atomic Layer Deposition: An Overview. *Chem. Rev.* **2010**, *110*, 111–131, doi:10.1021/cr900056b.
24. Sarakinos, K.; Alami, J.; Konstantinidis, S. High Power Pulsed Magnetron Sputtering: A Review on Scientific and Engineering State of the Art. *Surface and Coatings Technology* **2010**, *204*, 1661–1684, doi:10.1016/j.surfcoat.2009.11.013.
25. Arif, Md.F.H.; Ahmed, K.; Asaduzzaman, S.; Azad, Md.A.K. Design and Optimization of Photonic Crystal Fiber for Liquid Sensing Applications. *Photonic Sens* **2016**, *6*, 279–288, doi:10.1007/s13320-016-0323-y.
26. Van Newkirk, A.; Antonio-Lopez, E.; Salceda-Delgado, G.; Amezcua-Correa, R.; Schülzgen, A. Optimization of Multicore Fiber for High-Temperature Sensing. *Opt. Lett.* **2014**, *39*, 4812, doi:10.1364/OL.39.004812.
27. Wierzba, P.; Jędrzejewska-Szczerska, M. Optimization of a Fabry-Perot Sensing Interferometer Design for an Optical Fiber Sensor of Hematocrit Level. *Acta Physica Polonica A* **2013**, *124*, 586–588, doi:10.12693/APhysPolA.124.586.
28. Wang, Q.; Wei, W.; Guo, M.; Zhao, Y. Optimization of Cascaded Fiber Tapered Mach–Zehnder Interferometer and Refractive Index Sensing Technology. *Sensors and Actuators B: Chemical* **2016**, *222*, 159–165, doi:10.1016/j.snb.2015.07.098.
29. Azad, S.; Sadeghi, E.; Parvizi, R.; Mazaheri, A.; Yousefi, M. Sensitivity Optimization of ZnO Clad-Modified Optical Fiber Humidity Sensor by Means of Tuning the Optical Fiber Waist Diameter. *Optics & Laser Technology* **2017**, *90*, 96–101, doi:10.1016/j.optlastec.2016.11.005.
30. Mishra, A.K.; Mishra, S.K.; Gupta, B.D. SPR Based Fiber Optic Sensor for Refractive Index Sensing with Enhanced Detection Accuracy and Figure of Merit in Visible Region. *Optics Communications* **2015**, *344*, 86–91, doi:10.1016/j.optcom.2015.01.043.
31. Song, N.; Cai, W.; Song, J.; Jin, J.; Wu, C. Structure Optimization of Small-Diameter Polarization-Maintaining Photonic Crystal Fiber for Mini Coil of Spaceborne Miniature Fiber-Optic Gyroscope. *Appl. Opt.* **2015**, *54*, 9831, doi:10.1364/AO.54.009831.
32. Tu, M.H.; Sun, T.; Grattan, K.T.V. Optimization of Gold-Nanoparticle-Based Optical Fibre Surface Plasmon Resonance (SPR)-Based Sensors. *Sensors and Actuators B: Chemical* **2012**, *164*, 43–53, doi:10.1016/j.snb.2012.01.060.
33. Weber, M.; Kim, J.-Y.; Lee, J.-H.; Kim, J.-H.; Iatsunskyi, I.; Coy, E.; Miele, P.; Bechelany, M.; Kim, S.S. Highly Efficient Hydrogen Sensors Based on Pd Nanoparticles Supported on Boron Nitride Coated ZnO Nanowires. *J. Mater. Chem. A* **2019**, *7*, 8107–8116, doi:10.1039/C9TA00788A.
34. Graniel, O.; Weber, M.; Balme, S.; Miele, P.; Bechelany, M. Atomic Layer Deposition for Biosensing Applications. *Biosensors and Bioelectronics* **2018**, *122*, 147–159, doi:10.1016/j.bios.2018.09.038.
35. Viter, R.; Chaaya, A.A.; Iatsunskyi, I.; Nowaczyk, G.; Kovalevskis, K.; Erts, D.; Miele, P.; Smyntyna, V.; Bechelany, M. Tuning of ZnO 1D Nanostructures by Atomic Layer Deposition and Electrospinning for Optical Gas Sensor Applications. *Nanotechnology* **2015**, *26*, 105501, doi:10.1088/0957-4484/26/10/105501.

36. Elias, J.; Utke, I.; Yoon, S.; Bechelany, M.; Weidenkaff, A.; Michler, J.; Philippe, L. Electrochemical Growth of ZnO Nanowires on Atomic Layer Deposition Coated Polystyrene Sphere Templates. *Electrochimica Acta* **2013**, *110*, 387–392, doi:10.1016/j.electacta.2013.04.168.
37. Listewnik, P.; Bechelany, M.; Jasinski, J.B.; Szczerska, M. ZnO ALD-Coated Microsphere-Based Sensors for Temperature Measurements. *Sensors* **2020**, *20*, 4689, doi:10.3390/s20174689.